Ultra-Widefield Optical Coherence Tomographic Imaging of Posterior Vitreous in Eyes With High Myopia

HIROYUKI TAKAHASHI, NORIKO TANAKA, KOSEI SHINOHARA, TAE YOKOI, TAKESHI YOSHIDA, KENGO URAMOTO, AND KYOKO OHNO-MATSUI

• PURPOSE: To investigate the morphological changes of posterior vitreous in highly myopic (HM) eyes of patients 50 years of age and older.
• DESIGN: Retrospective, observational case series.
• METHODS: Ultra-widefield swept-source OCT (UWF-OCT) examinations were performed on 768 eyes of 448 HM patients (50-89 years of age) and 54 eyes of 52 non-HM subjects with scan widths of 23 mm and depths of 5 mm. HM was defined as an axial length longer than 26.5 mm. The area and morphology of the posterior vitreous detachments (PVDs) and adhesions onto retinal vessels were examined for in 167 HM eyes and in 11 non-HM eyes in which the vitreal images were clear.
• RESULTS: Paramacular PVD, perifoveal PVD, peripapillary PVD, and complete PVD were found in 9%, 47%, 41%, and 3% of the 167 HM eyes, respectively, and in 37%, 45%, 18%, and 0% of the 11 non-HM eyes, respectively. In eyes with vitreofoveal adhesions, the PVDs were more commonly asymmetrical relative to the fovea in the HM eyes than in the non-HM eyes (94% vs. 44%, respectively; $P < .001$). The area of the PVD corresponded with the area where the sclera protruded posteriorly. A thickened vitreous was observed to adhere to the retinal vessels at multiple points and was accompanied by paravascular abnormalities including lamellar holes in HM eyes. A total of 54 of the 167 HM eyes had macular retinoschisis, and the eyes commonly had vitreal traction on retinal vessels compared to HM eyes without macular retinoschisis ($P = .031$).
• CONCLUSIONS: PVD progressed asymmetrically and were associated with scleral curvature in HM eyes. Vitreous traction spanning a wide distance may lead to myopic traction maculopathy. (Am J Ophthalmol 2019;206:102–112. © 2019 Elsevier Inc. All rights reserved.)

AJO.com Supplemental Material available at AJO.com.
Accepted for publication Mar 7, 2019.

From the Department of Ophthalmology and Visual Science (H.T., N.T., K.S., T.Yok., T.Yosh., K.U., K.O.-M.), Tokyo Medical and Dental University Graduate School of Medical and Dental Sciences, Tokyo, Japan.

Inquiries to Kyoko Ohno-Matsui, Department of Ophthalmology and Visual Science, Tokyo Medical and Dental University, 1-5-45 Yushima, Bunkyo-ku, Tokyo, 113-8519, Japan; e-mail: k.ohno.oph@tmd.ac.jp

SLIT-LAMP EXAMINATIONS OF HIGHLY MYOPIC (HM) eyes show vitreous liquefaction at an early age, and a posterior vitreous detachment (PVD) is generally detected at a younger age in HM eyes than in non-myopic eyes.[1–4] However, frequent discrepancies between the preoperative slit-lamp findings and the intraoperative findings can be detected for the vitreous in HM eyes. Vitreous surgeons frequently encounter a membranous structure on the retina in eyes with myopic traction maculopathy despite the presence of an apparent PVD with Weiss ring.

Swept-source optical coherence tomography (OCT), and enhanced vitreous imaging has enabled clinicians to view the vitreoretinal interface with improvements in depth of view, which allows analyzing the microstructures of the vitreous cortex in detail.[5–7] Itakura and associates[8] examined HM eyes by swept source OCT and reported that PVDs were present more often in younger patients than in the non-HM eyes of controls. In addition, the HM eyes had a residual vitreous cortex that adhered to the surface of the retina more frequently than in control eyes. Wang and associates[9] reported the presence of expanding posterior precortical vitreous pockets in HM eyes, observed by using enhanced vitreous imaging by spectral domain OCT. However, the images obtained by these conventional OCT instruments covered only a small area of the vitreoretinal interface because of the relatively short scan lengths. Thus, the vitreoretinal interface could not be completely imaged especially in the peripheral areas. In addition, only the vitreous anterior to the retina could be examined because of the limited depth of the scans of the conventional OCT devices.

A prototype ultra-widefield swept source OCT (UWF-OCT) device has been developed that can analyze a region of interest of up to 23 × 20 mm and a depth of 5 mm. The present authors recently investigated 136 eyes with myopic macular retinoschisis (MRS) by using UWF-OCT and reported that the eyes with inner retinoschisis had an inward-directed tractional force that was related to vitreoretinal adhesions.[10] These findings suggested that pathologically altered vitreous in HM eyes may play an important role in the development of MRS.

The purpose of this study was to analyze the vitreous cortex and vitreoretinal interface in HM eyes to determine how the vitreous was altered in relation to the retina in HM eyes. In addition, a spatial relationship between the

0002-9394/$36.00
https://doi.org/10.1016/j.ajo.2019.03.011

vitreal changes and staphylomas and adhesions onto retinal vessels were analyzed. Based on the findings, possible mechanisms that lead to MRS are presented.

SUBJECTS AND METHODS

THIS WAS A RETROSPECTIVE OBSERVATIONAL CASE SERIES. The procedures were approved by the Ethics Committee of the Tokyo Medical and Dental University (TMDU), and they conformed to tenets of the Declaration of Helsinki. Signed informed consent was obtained from all participants.

This study included HM patients who were consecutively examined by UWF-OCT in the High Myopia Clinic at TMDU between February 2017 and February 2018. HM was defined as an axial length longer than 26.5 mm. For control subjects, the data of non-HM patients who were examined by UWF-OCT between February 2017 and February 2018 were analyzed. These control eyes were the fellow eyes of the patients with an epiretinal membrane or non-HM fellow eyes of the patients with unilateral HM. The exclusion criteria were presence of retinal diseases other than those with macular complications of pathologic myopia, a history of vitreoretinal surgery, and poor quality OCT images. Patients younger than 50 years of age also were excluded.

All participants underwent a comprehensive ocular examination including measurements of the refractive error (spherical equivalent) and axial length (IOL Master; Carl Zeiss Meditec, Jana, Germany), dilated stereoscopic fundus examinations, and 200Tx model scanning laser ophthalmoscopy (Optos PLC, Dunfermline, United Kingdom).

• **ULTRA-WIDEFIELD SWEPT SOURCE OCT EXAMINATIONS:** UWF-OCT images were obtained with a prototype UWF-OCT instrument (Canon Corp., Tokyo, Japan) with an A-scan repetition rate of 100,000 Hz. The light source was a tunable laser centered at 1,050 nm with a 100-nm tuning range. The length of the scanned line was 23 mm in the horizontal direction and 20 mm in the vertical direction. The scan depth was 5 mm. Cross-sectional scans centered on the fovea, and the automatic image averaging was set at 20 images. The map scans centered on the midpoint between the fovea and the optic disc and consisted of 256 single horizontal scans in the region of interest. Three-dimensional images of the posterior pole were reconstructed from the map scans by using ImageJ software (National Institutes of Health, Bethesda, Maryland).

The presence and extent of a posterior staphyloma were determined by UWF-OCT findings as described in detail by Shinohara and associates.[11] The edges of the staphyloma were defined by 2 consistent OCT features: a gradual thinning of the choroid from the periphery toward the staphyloma edge with a gradual rethickening of the choroid from the staphyloma edge toward the posterior pole, and an inward protrusion of the sclera at the staphyloma edge. Staphylomas were divided into 6 types, as follows: wide macular, narrow macular, peripapillary, nasal, inferior, and others. This classification was based on the results of the study by Ohno-Matsui[12] and a slight modification of the original classification by Curtin.[13]

• **EVALUATION OF POSTERIOR VITREOUS:** UWF-OCT images of the posterior vitreous were classified according to the presence of a PVD (eg, no PVD, partial PVD, and complete PVD). The degree of the partial PVD was divided into 4 groups based on the location of the PVD: paramacular PVD, in which the posterior vitreous was detached from the retina away from the macula but attached within the macular region; a perifoveal PVD, in which the posterior vitreous was detached from the retina within the macular region but attached to the retina at the fovea; a peripapillary PVD, in which the posterior vitreous was detached from the retina except at the optic disc; and a complete PVD, in which the posterior vitreous was detached from both the macula and optic disc but was adherent to the peripheral retina. The incidence of the different types of PVD was evaluated for each quadrant of the eyes with a vitreofoveal adhesion (ie, paramacular PVD and perifoveal PVD). Eyes whose PVDs were symmetrical with respect to the fovea were defined as "symmetrical PVD," whereas PVDs that were asymmetrical with respect to the fovea were defined as "asymmetrical PVDs."

Vitreoretinal images were analyzed by 2 masked observers (H.T. and K.O.M.), and the type of PVD was classified independently. When the decision was not the same, the 2 graders discussed the appearances that made their choice, and a final consensus was reached for all eyes. The vitreoretinal interface was examined, and the presence of retinal vessel traction, paravascular abnormalities such as paravascular retinal cysts, paravascular lamellar holes, and vascular microfolds were determined based on a complete agreement of the 2 observers.

The presence of MRS was determined from the UWF-OCT images. An MRS was defined as a splitting of the inner or outer retinal layer. The authors determined whether MRS was present in the macular area in the UWF-OCT images. They were identified as a circular area centered on the fovea with a diameter of 6 mm.

Statistical analyses were performed by using the SPSS version 24.0 software (SPSS, Chicago, Illinois, USA). The significance of the differences in characteristics between the 2 groups was determined by Student t tests, Mann-Whitney U tests, or Fisher exact possibility tests. A P value of <0.05 was considered statistically significant.

TABLE 1. Demographics of Highly Myopic Patients and Normal Subjects Who Underwent Ultra-Widefield Optical Coherence Tomographic Imaging

	Highly Myopic Patients	Non-Highly Myopic Patients	*P* Value
Number of eyes (no. of patients)[a]	768 (448)	54 (52)	
Men	119	4	.003
Women	329	48	
Age (y)[b]			
Mean ± SD	66 ± 9	71 ± 9	.001
Range	50-89	51-86	
Refractive error (diopter)			
Mean ± SD	−13.7 ± 4.3	−2.8 ± 2.5	<.0001
Range	−8.25 to −27	+1.9 to −7.9	
Mean axial length ± SD (mm)			
Mean ± SD	30.3 ± 2.0	24.6 ± 1.1	<.0001
Range	26.7-36.5	22.6-26.4	
Posterior staphyloma, n (%)[c]	104 (62)	0 (0)	
Staphyloma type, n (%)[d]			
Wide, macular	51 (49)	0	
Narrow, macular	45 (43)	0	
Peripapillary	0 (0)	0	
Nasal	1 (1)	0	
Inferior	0 (0)	0	
Other	7 (7)	0	

SD = standard deviation.

[a]*P* value was obtained by Fisher exact probability test.

[b]*P* value was obtained by Student *t* test.

[c]Posterior staphyloma is investigated for 167 highly myopic eyes who underwent posterior vitreous imaging.

[d]See Subjects and Methods for the classification of posterior staphyloma types.

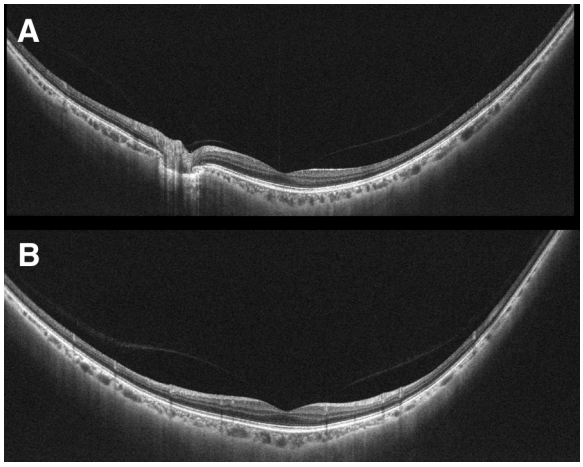

FIGURE 1. Ultra-widefield optical coherence tomographic images of a non-highly myopic eye. Left eye of a 52-year-old woman without retinal disease. The axial length of her left eye was 26.4 mm. Horizontal scan image with a length of 23 mm (A), and a vertical scan image with a length of 20 mm (B) shows perifoveal posterior vitreous detachment.

RESULTS

BETWEEN FEBRUARY 2017 AND FEBRUARY 2018, 664 PATIENTS were examined by UWF-OCT in the Department of Ophthalmology and Visual Science at TMDU. A total of 143 of the 664 patients were excluded because they were younger than 50 years of age. Among the remaining 521 patients, 94 eyes of 80 patients were excluded because of a history of vitreoretinal surgeries for rhegmatogenous retinal detachment or myopic traction maculopathy; 24 eyes of 17 patients because of poor quality UWF-OCT images; and 98 eyes of 69 patients because of the presence of other retinal diseases. In the end, 768 eyes of 448 highly myopic patients (the HM group) and 54 eyes of 52 patients with mild or no myopia (non-HM group) constituted the control group.

The mean age of the 448 patients in the HM group was 66 ± 9 years, ranging from 50 to 89 years of age, which was significantly younger than the 52 patients of the non-HM group with a mean age of 71 ± 9 years and a range of 51 to 86 years ($P = 0.001$). The mean refractive error (spherical equivalent) of eyes in the HM group, except for the 354 pseudophakic and 14 aphakic eyes, was −13.7 ± 4.3 diopters (D) with a range of −8.25 to −27 D. These eyes were more myopic than the eyes in the non-HM group, except for 16 pseudophakic eyes, with mean refractive error of −2.8 ± 2.5 D and a range from +1.9 to −7.9 D. The mean axial length of eyes in the HM group was 30.3 ± 2.0 mm with a range from 26.7 to 36.5 mm, which was significantly longer than the axial lengths of the eyes in the non-HM group with mean axial length of 24.6 ± 1.1 mm and a range of 22.6 to 26.4 mm (Table 1).

The UWF-OCT images showed the posterior vitreous in 167 (22%) of the 768 HM eyes and 11 (20%) of the 54 non-HM eyes (Figures 1 and 2), and all these eyes showed partial or complete PVDs. Of the 167 HM eyes, 16 eyes (9%) had a paramacular PVD, 78 eyes (47%) had a perifoveal PVD, 68 eyes (41%) had a peripapillary PVD, and 5 eyes (3%) had a complete PVD. In the 11 non-HM eyes, 4 eyes (37%) had paramacular PVD, 5 eyes (45%) had perifoveal PVD, 2 eyes (18%) had peripapillary PVD, and no eyes had a complete PVD. The eyes in the HM group had more advanced PVD than eyes in the non-HM group ($P = 0.019$) (Table 2).

In the 167 HM eyes, 104 eyes (62%) had a posterior staphyloma. The types of staphylomas were the wide macular type in 51 (49%), narrow macular type in 45 (43%), nasal type in 1 (1%), and other types in 7 (7%). None of the patients had a peripapillary or an inferior staphyloma. Of the 96 eyes with staphylomas in the macula (ie, the wide macular and narrow macular staphyloma),

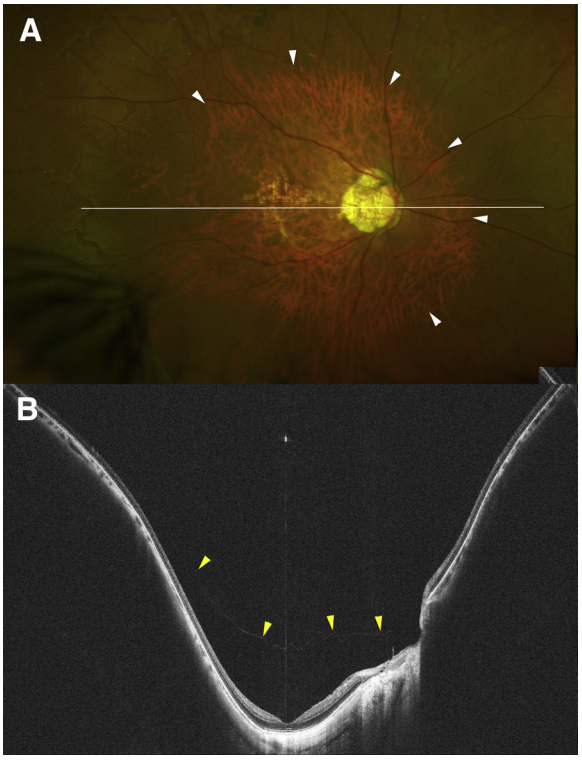

FIGURE 2. PVD restricted to the area of a staphyloma in an HM eye. (A) Fundus photograph of the left eye in a 57-year-old man with an axial length of 28.5 mm. The photograph shows a wide macular staphyloma (outlined by white arrowheads) and lacquer cracks in the macula. White long bar shows line scanned by the UWF-OCT instrument. (B). Horizontal UWF-OCT image showing a PVD (yellow arrowheads) within the staphylomatous area. PVD = posterior vitreous detachment; HM = highly myopic; UWF-OCT = ultra-widefield optical coherence tomography.

TABLE 2. Comparison of Ultrawide-Field OCT Findings Between Highly Myopic Patients and Normal Subjects Who Underwent Posterior Vitreous Imaging

	Highly Myopic Patients	Non-Highly Myopic Patients	*P* Value
Number of eyes	167	11	
Degree of PVD, n (%)[a]			
Paramacular PVD	16 (9)	4 (37)	
Perifoveal PVD	78 (47)	5 (45)	.019
Peripapillary PVD	68 (41)	2 (18)	
Complete PVD	5 (3)	0 (0)	
Vitreofoveal adhesion, n (%)[b]			
Number of eyes	94	9	
Symmetrical PVD	6 (6)	5 (56)	<.001
Asymmetrical PVD	88 (94)	4 (44)	
Retinal vessel traction, n (%)[b]	84 (50)	1 (9)	.01
Vascular microfold, n (%)[b]	114 (68)	1 (9)	<.001
Paravascular cystic lesion, n (%)[b]	80 (48)	1 (9)	.01
Paravascular lamellar hole, n (%)	20 (12)	0 (0)	
Multiple PVD, n (%)	15 (9)	0 (0)	
Multilayered PVD, n (%)	12 (7)	0 (0)	
Long vitreous strand, n (%)	32 (19)	0 (0)	

PVD = posterior vitreous detachment.
[a]*P* value was obtained by Mann-Whitney *U* test.
[b]*P* value was obtained by Fisher exact probability test.

a perifoveal PVD was more common than in the 63 eyes without a staphyloma (55% vs. 30%, respectively; $P = 0.008$). In addition, the PVD was restricted to the area within the staphyloma in 80 of the 104 eyes (77%) with a staphyloma (Figure 2).

The PVD was symmetrical in 5 (56%) of the 9 non-HM eyes with vitreofoveal adhesions, which was significantly higher than the 6 (6%) of 94 HM eyes with vitreofoveal adhesions ($P < 0.001$). Thus, 88 (94%) of the HM eyes had an asymmetrical PVD (Figure 3). Of these, 26 eyes had an asymmetrical PVD in the horizontal direction, 35 eyes had asymmetrical PVD in the vertical direction, and 27 eyes had asymmetrical PVD in both the horizontal and vertical directions. Among the 53 eyes with asymmetrical PVD in the horizontal direction, 42 eyes had a PVD only temporal to the fovea, and the other 11 eyes had PVD only nasal to the fovea. In 23 eyes with an asymmetrical PVD temporal to the fovea, the area of the PVD corresponded to the area where the sclera protruded posteriorly (Figure 3). On the other hand, among the 62 eyes with asymmetrical PVD in the vertical direction, 37 eyes had PVD only inferior to the fovea, and the other 25 eyes had PVD only superior to the fovea. In 17 eyes with an inferior PVD, the area of the PVD corresponded to the area where the sclera protruded posteriorly.

A thickened vitreous cortex was observed in the UWF-OCT images as a hyperreflective membranous tissue (Figure 4). The posterior surface of the vitreous cortex was seen to be adhered to the retinal vessels in 84 (50%) of the 167 HM eyes, and in only 1 (9.1%) of 11 non-HM eyes ($P = 0.01$). The retinal vessels were lifted anteriorly by the posterior vitreous cortex at the sites of the adhesions (Figure 4).

Vascular microfolds and paravascular retinal cysts were observed significantly more frequently in HM eyes than in non-HM eyes (114 of the 167 eyes [68.3%] vs. 1 of the 11 eyes [9%], respectively, and 80 of 167 eyes [47.9%] vs. 1 of 11 eyes [9%], respectively; $P < 0.001$ and $P = 0.01$, respectively). Paravascular lamellar holes were present in 20 (12%) of the 167 HM eyes and in none of the 11 non-HM eyes. Inner or outer retinoschisis was also found around lifted retinal vessels in 52 (62%) of the 84 HM eyes with retinal vessel traction.

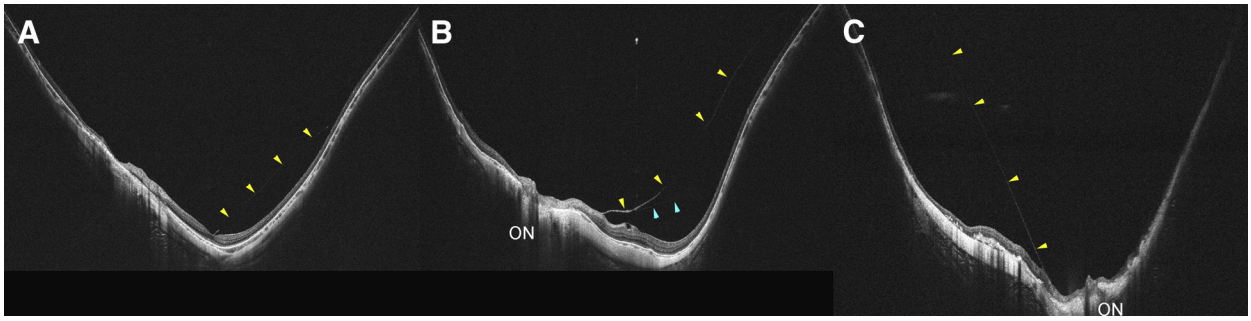

FIGURE 3. Asymmetrical PVD in HM eyes. (A). UWF-OCT image of the eye in a 57-year-old man with an axial length of 30.22 mm with a perifoveal PVD asymmetrical to the fovea. Posterior vitreous cortex is separated from the retina only temporal to the fovea (yellow arrowheads). Sclera outpouches the most posteriorly temporal to the fovea. (B) UWF-OCT image in a 57-year-old woman with an axial length of 30.89 mm with an asymmetrical PVD (yellow arrowheads) only temporal to the optic nerve head. Another layer of vitreous cortex is separated posteriorly (light blue arrowheads). Sclera protrudes asymmetrically temporal to the fovea. (C). UWF-OCT image of the eye of a 60-year-old woman with an axial length of 32.91 mm with an asymmetrical PVD in the right eye only temporal to the optic disc. Sclera protrudes asymmetrically on the temporal side of the fovea. HM = highly myopic; PVD = posterior vitreous detachment; UWF-OCT = ultra-widefield optical coherence tomography.

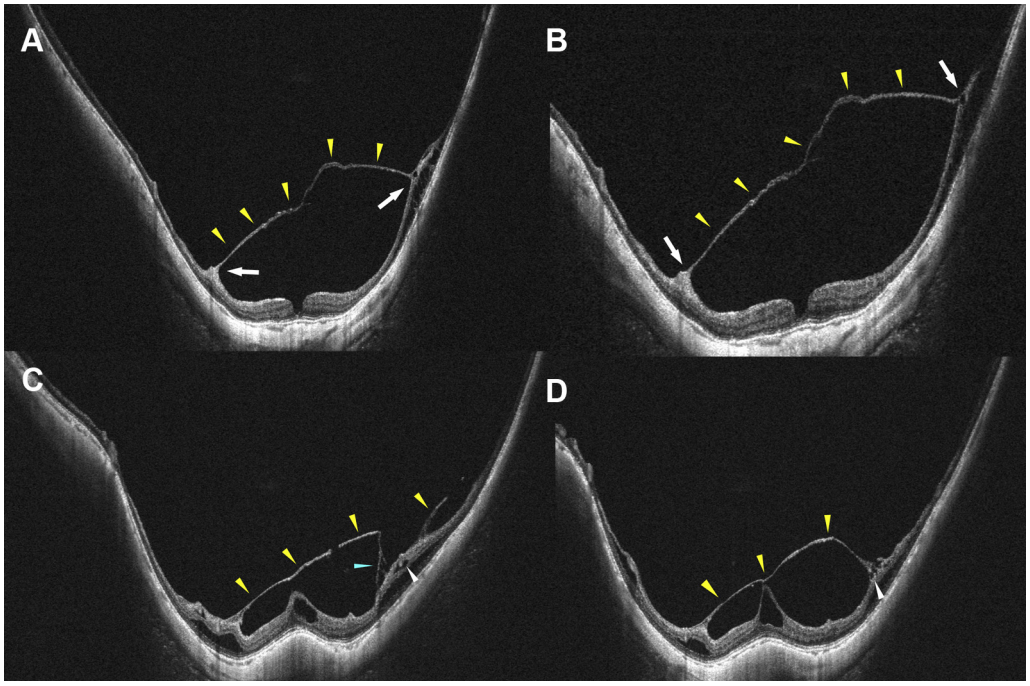

FIGURE 4. Thickened vitreous cortex adhering to retinal vessels at multiple points in HM eyes. (A and B) Sequential radial sections of UWF-OCT scans of the right eye of an 80-year-old woman. Vitreous cortex (yellow arrowheads) is adherent to the inner surface of retina. A close observation shows vitreous is adhered to the retinal vessels (arrows). Retinoschisis is seen around the adhesion site of the vitreous. A macular hole is present. (C and D) Sequential radial sections of UWF-OCT images of the left eye in a 67-year-old woman with an axial length of 30.53 mm. Vitreous cortex (yellow arrowheads) is adherent to the inner surface of the retina at multiple points including the fovea. Retinal vessels are lifted up anteriorly with the development of paravascular cystic lesion (white arrowhead). Vitreofoveal traction is seen in this eye with a dome-shaped macula. (C) Some of the membranous tissue extends from the inner retinal surface and connect to the thickened vitreous cortex (light blue arrowhead). HM = highly myopic.

Multiple PVDs with the posterior vitreous adhered to the inner retinal surface at multiple points were observed in 15 of the 167 HM eyes (Figure 5). Observations of serial OCT sections showed that the borders of the multiple PVDs corresponded to the sites of vitreous adhesions onto the retinal vessels in 11 eyes of these 15 eyes. Multilayered

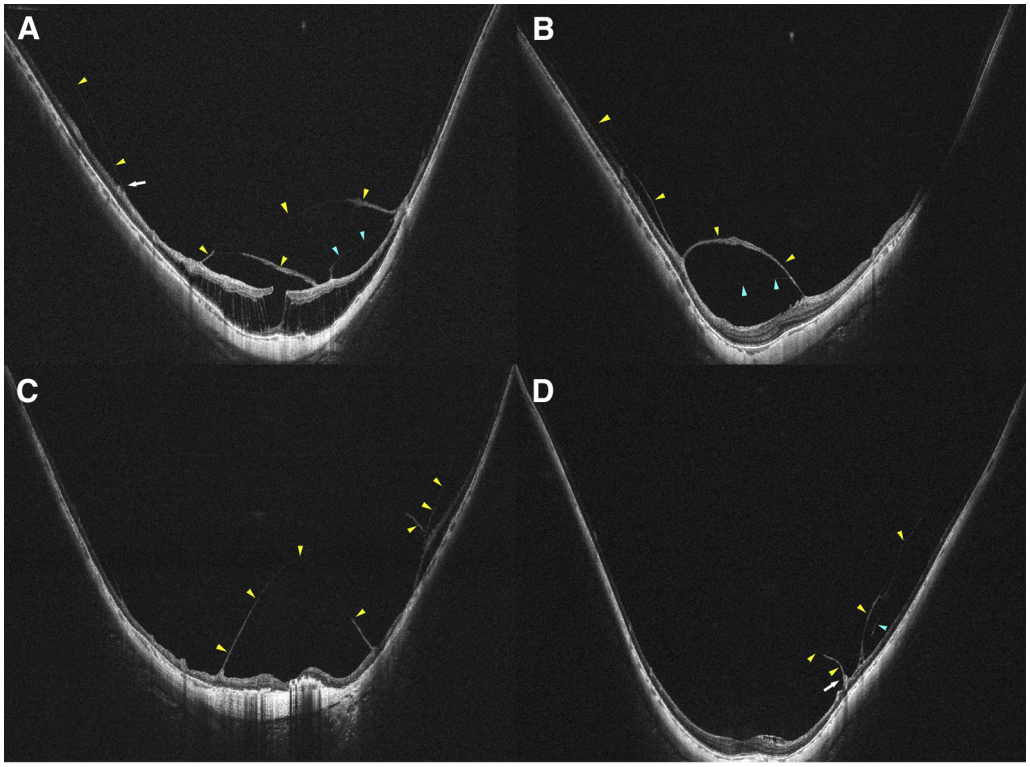

FIGURE 5. Multiple and multilayered PVDs in HM eyes. (A) UWF-OCT image of the eye of a 57-year-old woman with an axial length of 31.18 mm. Thickened vitreous cortex with nonuniform thickness (yellow arrowheads) is adherent to the inner surface of retina at multiple points. The border of the multiple PVDs corresponds to retinal vessels (white arrows). Outer retinoschisis can also be seen. Posterior to one layer of the PVD (yellow arrowheads), another layer of vitreous cortex can be seen separated from the retinal surface (light blue arrowheads). (B) UWF-OCT image of the eye of a 58-year-old woman with an axial length of 30.14 mm. Thickened vitreous cortex is adherent to the inner surface of the retina at multiple points (yellow arrowheads). Posterior to one layer of PVD (yellow arrowheads), another layer of vitreous cortex is also seen separated from the retinal surface (light blue arrowheads). (C) UWF-OCT image of the eye of a 60-year-old woman with an axial length of 32.91 mm and with a scar form of myopic choroidal neovascularization. Multiple PVDs are seen (yellow arrowheads). On the right side, the inner retina is lifted at the adhesion to the vitreous and retinoschisis is seen. (D) UWF-OCT image of the eye of a 69-year-old man with an axial length of 32.57 mm. The vitreous cortex is adherent to the inner surface of the retina inferior to the fovea (yellow arrowheads). The border of PVD corresponds to a retinal vessel (white arrow). At the inferior peripheral fundus, the vitreous cortex is separated into two layers (light blue arrowhead). HM = highly myopic; PVD = posterior vitreous detachment; UWF-OCT = ultra-widefield optical coherence tomography.

PVDs were also observed in 12 of 167 HM eyes (Figure 5). In these 12 eyes, 11 eyes had sites where the retinal vessels were lifted by the posterior vitreous cortex.

In 32 HM eyes, unusually long strands of posterior vitreous were observed (Figure 6). These strands adhered to retinal vessels and ran a long distance anteriorly without attaching to any other structures in the peripheral retina in the 23-mm-wide and 5-mm-deep UWF-OCT images. Thus, these strands appeared to be "floating" from retinal vessels anteriorly (Figure 6). In 14 of these 32 eyes with the long strands, the retinal vessels and the retinal tissue were lifted by these strands (Figure 6F). Eighteen of these 32 eyes had a posterior staphyloma, and the other 14 eyes had no posterior staphyloma. Among the 18 eyes with a posterior staphyloma, 10 eyes had a PVD that expanded out of the staphyloma, and the other 8 eyes had a PVD within the staphyloma.

An MRS was observed in 54 of the 167 HM eyes (Figure 7), and the patients were younger and had shorter axial lengths, but their refractive errors were not significantly different than those without an MRS (Table 3). Fifty-four eyes with an MRS had posterior staphylomas, which was more than the 113 eyes without an MRS (41 of 54 eyes [76%] vs 63 of 113 eyes [56%], respectively; $P = 0.016$). In addition, the frequency of eyes with an adherence of the posterior vitreous to retinal vessels was higher in eyes with an MRS than without an MRS (34 of 54 eyes [63%] vs. 50 of 113 eyes [44%], respectively; $P = 0.031$). Paravascular abnormalities, except for vascular microfolds, were more commonly observed in eyes with an

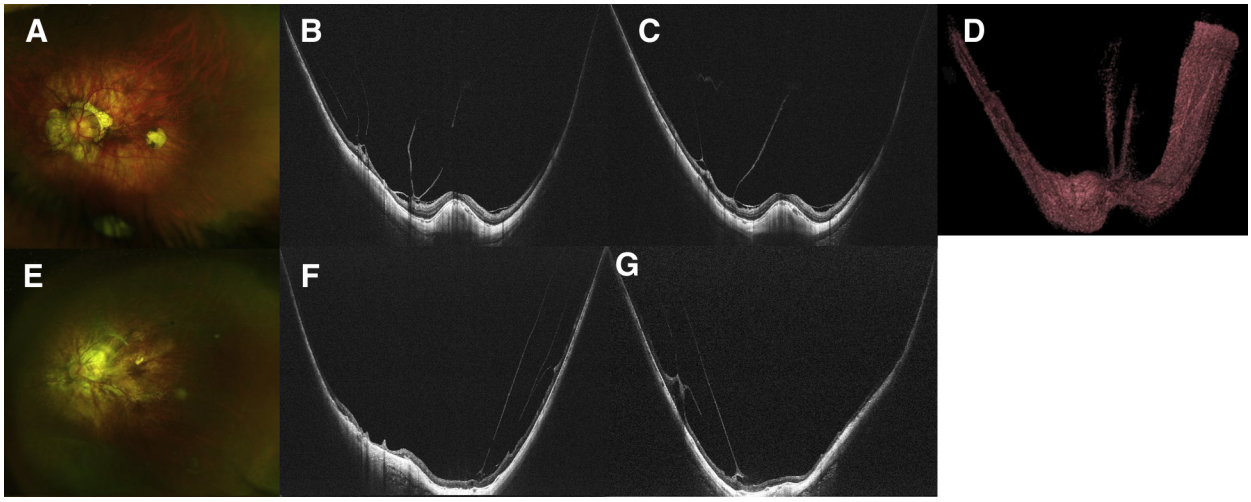

FIGURE 6. Unusually long strands of posterior vitreous cortex in HM eyes. (A) Left fundus of the eye of a 56-year-old man with an axial length of 31.1 mm showing diffuse chorioretinal atrophy. (B). Sequential radial sections of UWF-OCT show long vitreous strands running anteriorly from the retinal surface. These strands adhere to the retinal vessels at multiple points and appear to be floating without adhering to the peripheral fundus. (C) Three-dimensional image of long strands of posterior vitreous. The spatial relationship between the elongated eye shape and long vitreous strands running in the eye is clearly seen. (D) Left fundus of the eye of a 76-year-old man with an axial length of 33.2 mm showing diffuse chorioretinal atrophy. (E, F) Sequential radial sections of UWF-OCT showing two long vitreous strands running anteriorly from the retinal surface in parallel. These strands adhere to the retinal vessels at multiple points and lift the retinal tissues anteriorly. HM = highly myopic; UWF-OCT = ultra-widefield optical coherence tomography.

MRS than in those without an MRS. Paravascular retinoschisis was observed more frequently in eyes with an MRS than in those without an MRS. The presence of multiple PVDs, multilayered PVDs, and long strands of vitreous was not significantly different between eyes with and without an MRS (Table 3).

DISCUSSION

THE IMAGES OF THE VITREOUS OBTAINED BY NEWLY developed UWF-OCT were able to show the posterior hyaloid and its relationship to the retina in a large number of HM eyes. Earlier slit-lamp observations showed an earlier liquefaction and a larger cistern of the vitreous in HM eyes than in non-HM eyes.[4,8,9] These earlier studies analyzed the vitreoretinal interface of HM eyes with conventional OCT instruments, and the findings showed larger empty spaces above the macula, the so-called premacular bursae.[8] However, these observations were limited to a limited area of the vitreoretinal interface, and the entire extent of the vitreal changes occurring over a wider and deeper range has not been reported. In addition to the wider and deeper range (ie, 23 × 20 mm wide and 5 mm deep), the swept source OCT enabled recording images of tissues at different depths from the vitreous to the sclera. Use of these features allowed obtaining images of the vitreous that could be analyzed, especially in HM eyes with long axial lengths deformed by posterior staphylomas. Viewing the vitreal changes together with the alterations of the scleral curvature including the staphylomas in HM eyes can provide the characteristics of the PVDs and provide important clues to the pathogenesis of MRS.

Advanced forms of PVDs were found more frequently in HM eyes than in non-HM eyes, even though HM subjects were significantly younger than the non-HM subjects. This supports the results of Itakura and associates.[8] In addition, the present study's results showed different types of vitreous abnormalities, most of which had not been reported in the earlier studies. PVDs that were asymmetrical to the fovea were found more commonly in HM eyes than in the non-HM control eyes. Tsukahara and associates[14] reported that a PVD occurred often in the superior quadrant of the fundus but that other quadrants were also involved in healthy eyes. They suggested that gravitational forces acted on the superior vitreous body and caused the superior PVD. Perifoveal PVDs were detected more frequently temporally and inferiorly to the fovea in the HM eyes. The present results showed that the locations of the asymmetrical PVDs corresponded to the sites where the sclera was displaced most posteriorly (ie, the regions of outpouching). This suggests that the asymmetrical PVDs in HM eyes may have occurred in parallel with the changes of the scleral curvature.

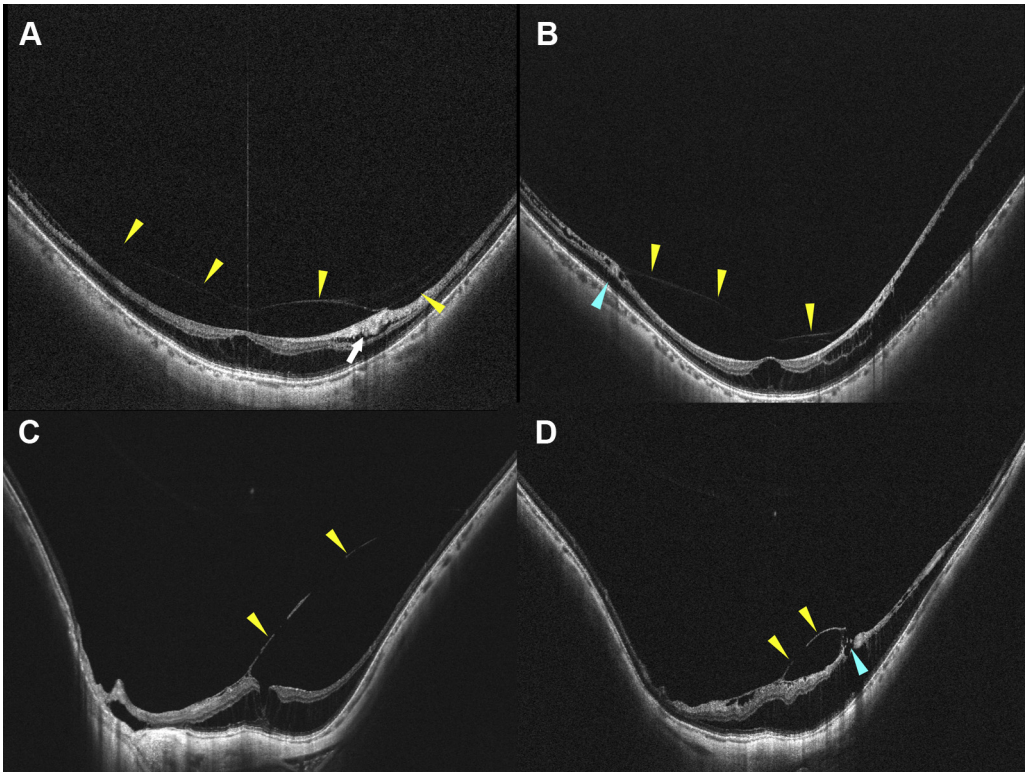

FIGURE 7. MRS in HM eyes. (A and B) Sequential radial sections of UWF-OCT images of the right eye of a 59-year-old man with an axial length of 28.2 mm. The vitreous cortex (yellow arrowheads) is separated from the inner surface of retina but adheres to the retinal vessels (arrow). (A) Retinoschisis is seen around the adhesion site of the vitreous and extends to the macular area, MRS. (B). Splitting of the outer retinal layer is more severe at the site of the vitreoretinal adhesion. (light blue arrowhead). (C and D). Sequential radial sections of UWF-OCT images of the left eye of a 65-year-old woman with an axial length of 32.25 mm. Thickened vitreous cortex (yellow arrowheads) is adherent to the fovea and retinal vessels. (D) A retinal vessel is lifted anteriorly at the site of adhesion with paravascular lamellar hole (light blue arrowhead) and splitting of the outer retinal layer extending to the macular area, MRS. HM = highly myopic; MRS = macular retinoschisis; UWF-OCT = ultra-widefield optical coherence tomography.

In HM eyes, the posterior vitreous was adherent to the inner retinal surface not only at the fovea but also at several points and appeared as "multiple PVDs" (Figure 5). The borders of such multiple PVDs corresponded to the retinal vessels. It is likely that the posterior vitreous moved during eye movements which would result in changing degrees of tractional force on the retinal vessels along with that on the surrounding inner retinal tissues. This is supported by the high incidence of vascular microfolds and paravascular retinal cysts on and around the retinal vessels to which the vitreous was attached. In some cases, a retinoschisis was observed around the lifted retinal vessels (Figure 4). These results suggested that strong tractional force due to vitreoretinal adhesion on the retinal vessels may be one of the causes of MRS as was suggested by Shimada and associates.[15]

In addition to the multiple PVDs, multilayered PVDs were also observed. The pathogenesis of the multilayered PVDs in HM eyes has not been well investigated, but they share some properties with vitreoschisis, a term coined by Balazs.[16] Sebag[17] described a vitreoschisis as a split of the posterior cortex that develops from anomalous PVDs. Considering the fact that asymmetrical PVDs were detected frequently in HM eyes, it is possible that the multilayered PVDs were caused by anomalous PVDs in HM eyes. However, multilayered PVDs extending over a wide range and connecting to retinal vessels have not been reported as characteristics of vitreoschisis and may be specific to HM eyes.

The vitreous cortex appeared thickened and was intensely reflective in the UWF-OCT images in HM eyes. This change has not been reported. Sakaguchi and associates[18] excised 3-layered membranes that were made visible by triamcinolone acetonide and indocyanine green staining during vitrectomy in a patient with a myopic macular hole retinal detachment. These membranes were tightly adherent to the retinal surface. Electron microscopy evaluation showed that the first layer consisted of acellular collagen fibers suggestive of the posterior vitreous, and the second layer was composed of parts of fibroblast-like cells

TABLE 3. Comparisons of Ultra-Widefield OCT Findings Between Highly Myopic Patients With and Without Macular Retinoschisis

	With Macular Retinoschisis	Without Macular Retinoschisis	*P* Value
Number of eyes	54	113	
Mean ± SD age (y)[a]	66 ± 8	63 ± 8	.04
Mean ± SD refractive error (diopter)[a]	-14.5 ± 1.2	-15.0 ± 4.8	.57
Mean ± SD axial length (mm)[a]	30.0 ± 1.6	30.9 ± 2.0	.006
Posterior staphyloma, n (%)[b]	41 (76)	63 (56)	.016
Retinal vessel traction, n (%)[b]	34 (63)	50 (44)	.031
Vascular microfolds, n (%)[b]	41 (76)	73 (65)	.16
Paravascular retinal cysts, n (%)[b]	38 (70)	42 (37)	<.001
Paravascular retinoschisis, n (%)[b]	21 (38)	19 (17)	<.001
Paravascular lamellar hole, n (%)[b]	11 (20)	9 (8)	.039
Multiple PVD, n (%)[b]	5 (9)	10 (9)	>.99
Multilayered PVD, n (%)[b]	5 (9)	7 (6)	.52
Long vitreous strands, n (%)[b]	12 (22)	20 (18)	.53

PVD = posterior vitreous detachment; SD = standard deviation.

[a]*P* value was obtained by Student *t* test.

[b]*P* value was obtained by Fisher exact probability test.

and collagen fibrils, suggesting a proliferative epiretinal membrane. The third layer was the internal limiting membrane. Yokota and associates[19] suggested that cells in the vitreous migrated through the paravascular margin of the thinner parts of the internal limiting membrane. These findings supported previous suggestions that the internal limiting membrane becomes thin and is sometimes absent over major retinal vessels and that the vitreous is attached to the retina at such areas.[20]

Some earlier studies[15,21–23] reported the presence of strong adhesion of vitreous to retinal vessels. Kishi and associates[23] examined the retinal surface of autopsied eyes by scanning electron microscopy and found that glial-like cells were often observed along retinal vessels. Spencer and associates[21] reported paravascular retinal rarefaction which was associated with an attached posterior vitreous. Results of the present study showed that the vitreous cortex lifted the retinal vessels and that paravascular abnormalities (eg, paravascular retinal cysts and paravascular lamellar holes) were found in these areas in some eyes. Thus, a strong traction of the vitreous on the retinal vessels might facilitate the migration of cells through the paravascular lesions and lead to a more proliferative and pathologic vitreous.

Unusually long vitreous strands were detected running almost perpendicularly from the retinal vessels anteriorly without attaching to anything in the periphery (Figure 6). These observations confirm earlier studies by conventional swept-source or spectral domain OCT that reported the presence of the vitreous cortex extending perpendicularly from the retinal surface.[8] However, the images were restricted to a narrow area anterior to the retinal surface because of the limited scan length of the conventional OCT instruments. Thus, the observation of such long vitreous strands became possible only with the UWF swept-source OCT device used in the present study. It seems reasonable that the traction on the retinal vessels by such long strands was very intense.

Figure 8 shows how and what kinds of vitreous changes occur in HM eyes in association with the changes that occur in the shape of the eyes and their spatial relationship with retinal vessels. In normal or mildly to moderately myopic eyes, the vitreous cortex separates from the retina at a paramacular area of the peripheral fundus and extends toward the perifoveal area and reaches the peripapillary area.[14] In HM eyes with asymmetrical eye shapes (eg, a temporally distorted eye) a PVD begins to develop in the area where the sclera is the most outpouched posteriorly. After the release of adhesion between vitreous cortex and retinal vessels, asymmetrical perifoveal PVDs are formed. In HM eyes with a posterior staphyloma, PVDs develop initially within the staphyloma area. The PVDs progress within the area of the staphyloma in accordance with irregular vitreoretinal adhesion which occasionally causes myopic traction maculopathy. After the release of vitreoretinal adhesions, PVDs develop completely only within the staphyloma. In severely elongated barrel-shape eyes, the PVD progresses with the irregular vitreoretinal adhesion at the sites of the retinal vessels. When the adhesions, except in the peripapillary area, are released, long vitreous strands extend perpendicularly from the retina. During this PVD progression, local adhesions between the vitreous and retinal vessel remain and could be the cause MRS through a traction on the inner retina.

The present results showed that paravascular abnormalities caused by vitreal adhesions and tractions on retinal vessels were found significantly more frequently in eyes with MRS than in those without MRS (Table 3). Shimada and associates[15] reported similar findings showing that paravascular lamellar holes and paravascular retinal cysts were found more often in eyes with MRS. In addition, results from the present study clearly showed that pathological vitreous changes and persistent adhesion of vitreous to retinal vessels might be the cause of intense traction on the retinal vessels which eventually results in the development of paravascular abnormalities.

There are limitations in this study. First, the possibility of referral bias might have existed because the present study did not have a population-based recruitment for its participants. Thus, it is not clear whether the results could be directly transferred to other HM groups in the general population. In addition, the number of control subjects was very small. Second, due to the retrospective observational

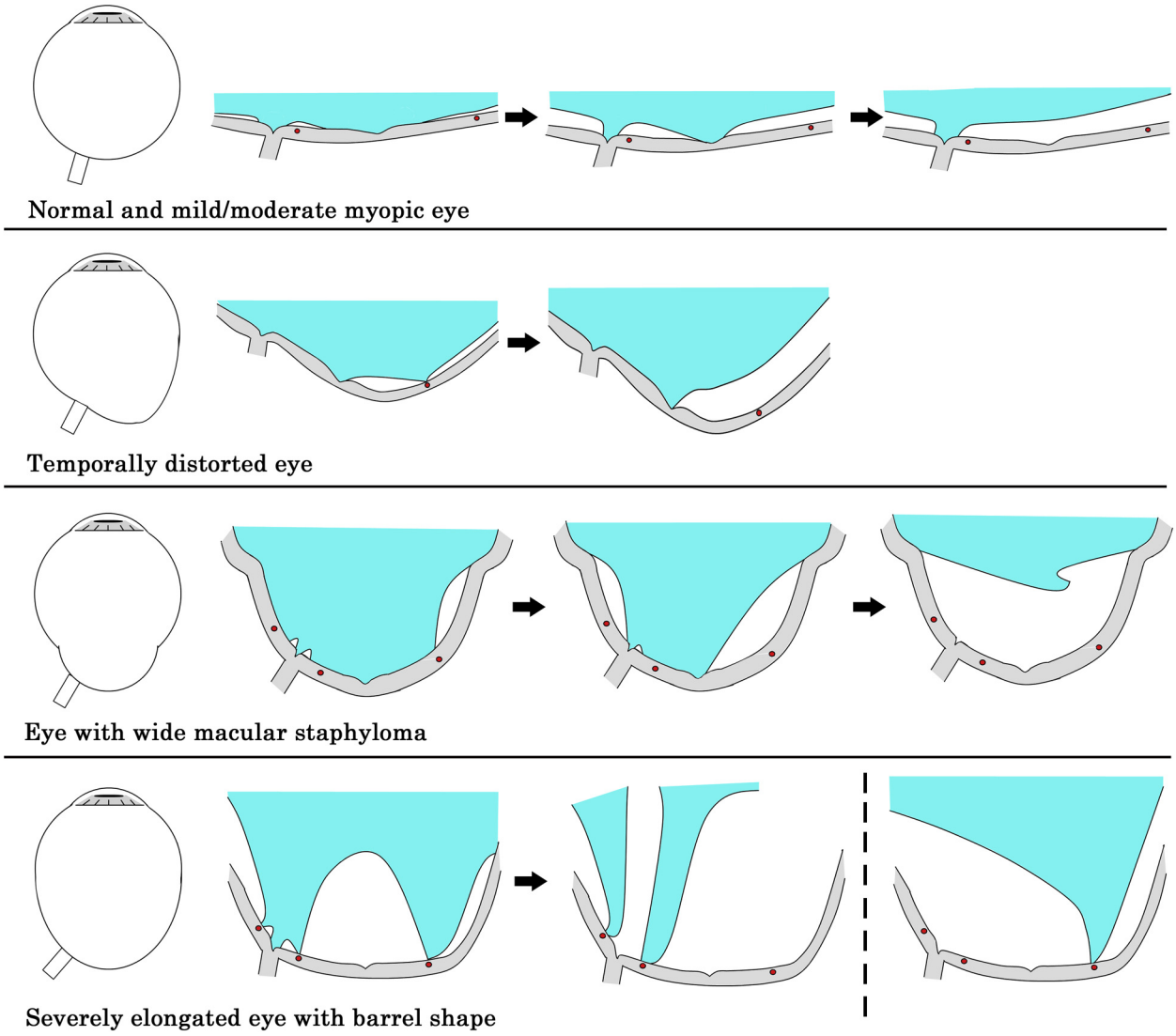

FIGURE 8. Schematic shows the course of PVDs in normal and HM eyes in association with eye shape changes and spatial relationship with the retinal vessels. In normal eyes, the vitreous separates from the retina at a paramacular area in the peripheral fundus, extends towards the perifoveal area and reaches the peripapillary area. In HM eyes with an asymmetrical shape (eg, a temporally distorted eye), the PVD begins to develop in the area where the sclera is most outpouched posteriorly. After the release of adhesion between vitreous cortex and retinal vessels, asymmetrical perifoveal PVD is formed. In HM eyes with posterior staphyloma, PVD developed initially within the staphyloma, progresses in accordance with the irregular vitreoretinal adhesion and develops completely only within the staphyloma. In severely elongated eyes with barrel shape, the PVD progresses, remaining as irregular vitreoretinal adhesion at the site of the retinal vessels. When the adhesions are released, long vitreous strands extend perpendicularly from retina except in the peripapillary area. Schema at bottom-right corner. Local adhesion between vitreous and retinal vessel remains and can cause macular retinoschisis through an intense traction on the inner retina. HM = highly myopic; UWF-OCT = ultra-widefield optical coherence tomography.

nature of this study, changes over time were not analyzed for each lesion. To confirm the pathophysiology of vitreous cortex and progression of vitreoretinal tractions in HM eyes, further long-term longitudinal studies are needed. Third, the posterior vitreous was visible in approximately 20% of HM eyes as well as in non-HM eyes, which was lower than the visibility rate in the earlier studies.[8,24] This may be because many of the patients whose vitreous was not visible might have had a complete PVD. In eyes with a complete PVD, it is assumed that posterior vitreous was not clearly visible with UWF-OCT because of liquefaction of vitreous as well as an increased movability of vitreous due to eye movement. In addition, it may be possible that the resolution of UWF-OCT might be lower than with commercially available OCT device, regarding the visibility of posterior vitreous.

However, with those caveats in mind, the authors conclude that UWF-OCT can obtain tomographic images of the posterior vitreous cortex with high resolution. UWF-OCT revealed unusual vitreal changes over a wide area and also showed the possibility of how such pathological vitreal changes can cause traction on the retinal vessels which could result in the development of MRS.

ACKNOWLEDGEMENTS

ALL AUTHORS HAVE COMPLETED AND SUBMITTED THE ICMJE FORM FOR DISCLOSURE OF POTENTIAL CONFLICTS OF INTEREST and none were reported. The authors indicate no financial conflict of interest. The authors thank Professor Emeritus Duco Hamasaki of the Bascom Palmer Eye Institute of the University of Miami for discussions and critical editing.

REFERENCES

1. Akiba J. Prevalence of posterior vitreous detachment in high myopia. *Ophthalmology* 1993;100(9):1384–1388.
2. Yonemoto J, Ideta H, Sasaki K, et al. The age of onset of posterior vitreous detachment. *Graefes Arch Clin Exp Ophthalmol* 1994;232(2):67–70.
3. Morita H, Funata M, Tokoro T. A clinical study of the development of posterior vitreous detachment in high myopia. *Retina* 1995;15(2):117–124.
4. Gale J, Ikuno Y. Myopic vitreopathy. In: Sebag J, ed. Vitreous—in Health and Disease. New York: Springer; 2014:113–130.
5. Liu JJ, Witkin AJ, Adhi M, et al. Enhanced vitreous imaging in healthy eyes using swept source optical coherence tomography. *PLoS One* 2014;9(7):e102950.
6. Stanga PE, Sala-Puigdollers A, Caputo S, et al. In vivo imaging of cortical vitreous using 1050-nm swept-source deep range imaging optical coherence tomography. *Am J Ophthalmol* 2014;157(2):397–404.
7. Spaide RF. Visualization of the posterior vitreous with dynamic focusing and window averaging swept source optical coherence tomography. *Am J Ophthalmol* 2014;158(6):1267–1274.
8. Itakura H, Kishi S, Li D, et al. Vitreous changes in high myopia observed by swept-source optical coherence tomography. *Invest Ophthalmol Vis Sci* 2014;55(3):1447–1452.
9. Wang X, Shen M, Wang R, et al. Posterior precortical vitreous pockets in high myopia observed by enhanced vitreous imaging of spectral domain optical coherence tomography. *Retina* 2019;39(6):1100–1109.
10. Shinohara K, Tanaka N, Jonas JB, et al. Ultrawide-field OCT to investigate relationships between myopic macular retinoschisis and posterior staphyloma. *Ophthalmology* 2018;125(10):1575–1586.
11. Shinohara K, Shimada N, Moriyama M, et al. Posterior staphylomas in pathologic myopia imaged by widefield optical coherence tomography. *Invest Ophthalmol Vis Sci* 2017;58(9):3750–3758.
12. Ohno-Matsui K. Proposed classification of posterior staphylomas based on analyses of eye shape by three-dimensional magnetic resonance imaging. *Ophthalmology* 2014;121(9):1798–1809.
13. Curtin BJ. Posterior staphyloma development in pathologic myopia. *Ann Ophthalmol* 1982;14(7):655–658.
14. Tsukahara M, Mori K, Gehlbach PL, et al. Posterior vitreous detachment as observed by wide-angle OCT imaging. *Ophthalmology* 2018;125(9):1372–1383.
15. Shimada N, Ohno-Matsui K, Nishimuta A, et al. Detection of paravascular lamellar holes and other paravascular abnormalities by optical coherence tomography in eyes with high myopia. *Ophthalmology* 2008;115(4):708–717.
16. Balazs EA. Fine structure and function of ocular tissues. The vitreous. *Int Ophthalmol Clin* 1973;13(3):169–187.
17. Sebag J. Vitreoschisis. *Graefes Arch Clin Exp Ophthalmol* 2008;246(3):329–332.
18. Sakaguchi H, Ikuno Y, Choi JS, et al. Multiple components of epiretinal tissues detected by triamcinolone and indocyanine green in macular hole and retinal detachment as a result of high myopia. *Am J Ophthalmol* 2004;138(6):1079–1081.
19. Yokota R, Hirakata A, Hayashi N, et al. Ultrastructural analyses of internal limiting membrane excised from highly myopic eyes with myopic traction maculopathy. *Jpn J Ophthalmol* 2018;62(1):84–91.
20. Sebag J. Vitreous and vitreoretinal interface. In: Schachat AP, ed. Ryan's Retina. 6th edition. Amsterdam: Elsevier; 2018:544–581.
21. Spencer LM, Foos RY. Paravascular vitreoretinal attachments. Role in retinal tears. *Arch Ophthalmol* 1970;84(5):557–564.
22. Foos RY. Vitreoretinal juncture over retinal vessels. *Albrecht Von Graefes Arch Klin Exp Ophthalmol* 1977;204(4):223–234.
23. Kishi S, Numaga T, Yoneya S, et al. Epivascular glia and paravascular holes in normal human retina. *Graefes Arch Clin Exp Ophthalmol* 1986;224(2):124–130.
24. Itakura H, Kishi S, Li D, et al. En face imaging of posterior precortical vitreous pockets pockets using swept-source optical coherence tomography. *Invest Ophthalmol Vis Sci* 2015;56(5):2898–2900.